Published in final edited form as:
*IEEE Sens J*. 2026 February 15; 26(4): 5327–5335. doi:10.1109/JSEN.2025.3645254.

# Development of a Disposable Chemiresistive Biochip for Tear-Based Retinopathy of Prematurity Diagnosis: Early Screening and Risk Prediction

**Tanmoya Nemai Ghosh**[1,*], **Saurabh Kumar**[2,3,*], **Subhadra Jalali**[4], **Aakash Belenje**[4], **Aatish Mahajan**[2], **Inderjeet Kaur**[2,#], **Shiv Govind Singh**[1,#]

[1]Department of Electrical Engineering, Indian Institute of Technology, Hyderabad, 502285, India.

[2]Prof. Brien Holden Eye Research Centre, L V Prasad Eye Institute, Hyderabad-500034

[3]Manipal Academy of Higher Education, Manipal, Karnataka, India, -576104

[4]Anant Bajaj Retina Institute, L V Prasad Eye Institute, Hyderabad-500034

## Abstract

Retinopathy of prematurity (ROP) is a dreadful eye condition and is considered as leading cause of blindness in children around the globe. Lack of timely and appropriate treatment for this ocular condition leads to abnormal development of retinal blood vessels and progression to the severe stage ROP, resulting in irreversible blindness. Based on our previous studies that identified matrix metalloproteinases (MMPs) to be potential tear biomarkers, herein we are demonstrating that the increased levels of MMP-9 in tears can help in ROP risk prediction. A biochip integrated with vanadium disulfide nanowires ($VS_2$NWs) and resistance measurement circuitry for quantitative analysis of MMPs was established. The biochip fabrication process was optimized using a hybrid central composite design (CCD)-support vector regression (SVR) method resulted in an enhanced signal amplification of the sensor output ($\Delta R/R$). The 30 preterm tear samples (10 healthy, 10 mild ROP and 10 severe ROP) were collected across the neonatal care units, and the tear MMPs were analyzed by the $VS_2$NW-based biochip and commercial ELISA kits. The $VS_2$NW biochip showed a similar inclination for the expression of MMP-2 and MMP-9 as seen using the commercial ELISA kits and exhibited an AUC of 0.9778 on the external test set, with 100% sensitivity and 96.67% specificity. This study proved the reliability of the $VS_2$NW biochip platform to identify ROP tear biomarkers and screen high-risk ROP babies in a quick and non-invasive manner.

[#]Corresponding Authors: Inderjeet Kaur - inderjeet@lvpei.org; Shiv Govind Singh - sgsingh@ee.iith.ac.in.
[*]Both Contributed Equally

Credit Authorship Contribution Statement

**Tanmoya Nemai Ghosh:** methodology; writing – original draft; validation; software; data curation; formal analysis; investigation. **Saurabh Kumar:** methodology; writing – original draft; validation; software; data curation; formal analysis; investigation. **Aakash Belenje:** formal analysis; investigation. **Subhadra Jalali:** formal analysis; investigation. **Aatish Mahajan:** writing – original draft; formal analysis; investigation. **Inderjeet Kaur:** Conceptualization; methodology; data curation; supervision; resources; project administration; validation; visualization; writing – review and editing; writing – original draft; funding acquisition; investigation. **Shiv Govind Singh:** Conceptualization; methodology; data curation; supervision; resources; project administration; validation; visualization; writing – review and editing; writing – original draft; funding acquisition; investigation.


Europe PMC Funders Author Manuscripts

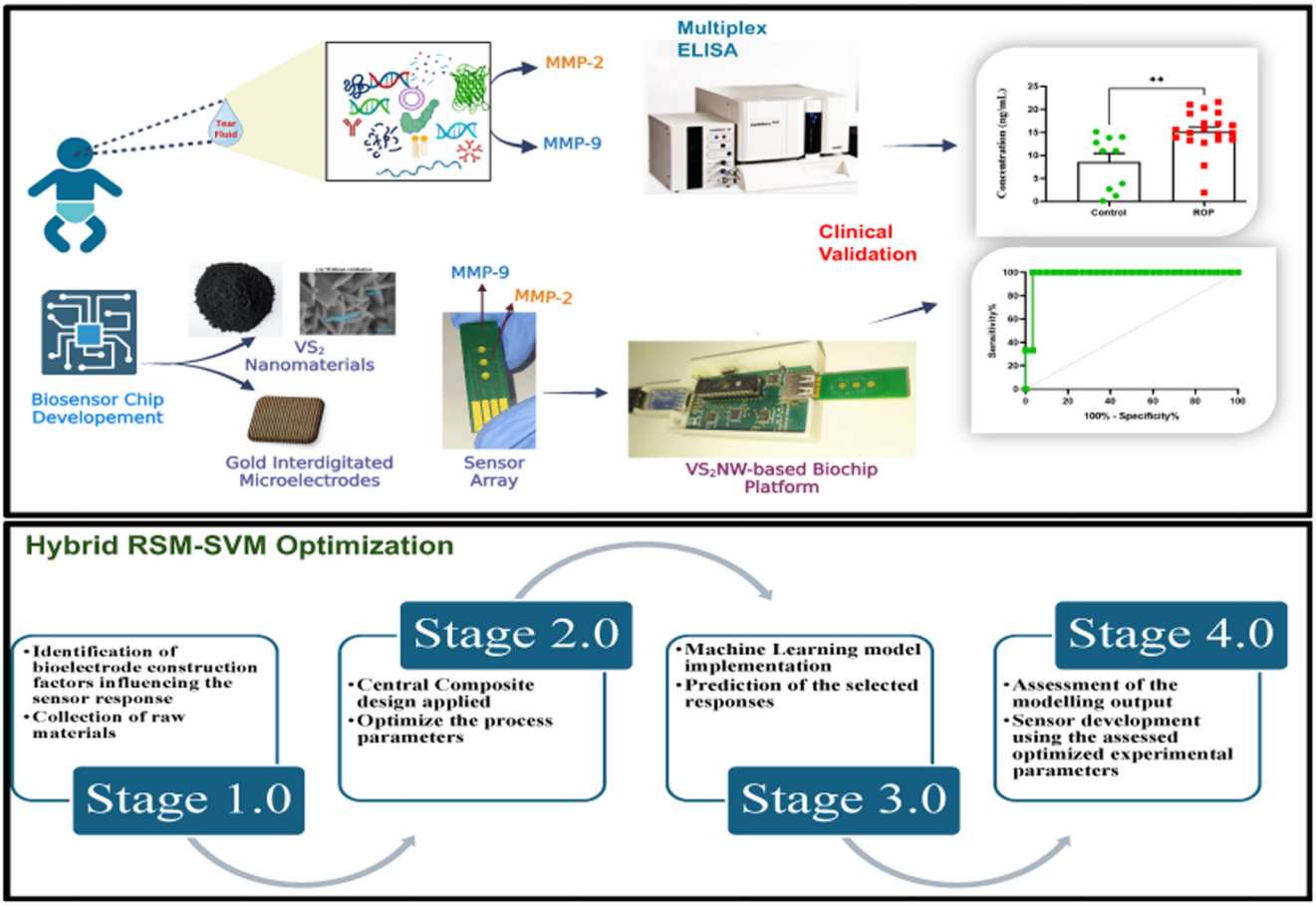


**Index Terms**

biosensor; matrix metalloproteinases; Retinopathy of prematurity; limit of detection; sensitivity

## I Introduction

**P**reterm-born infants are at risk of developing retinopathy of prematurity (ROP), characterized by neovascularization and neuroinflammation leading to blindness. About 10% to 18% of preterm infants born annually in high-income countries and up to 40% in low- and middle-income countries develop ROP, with approximately 18% of affected infants suffering from substantial vision loss [1], [2]. Preterm infants diagnosed with plus ROP, as marked by the growth of abnormal blood vessels on a partially avascular retina, are treated with laser therapy and/or anti-VEGF (Vascular Endothelial Growth Factor) therapy [3]. Currently available treatments for ROP focus mainly on reducing the disease's progression. Moreover, preterm infants who develop ROP are at greater risk for secondary eye conditions such as retinal detachment, glaucoma, strabismus, myopia, and amblyopia. It is also very unpredictable, as not every preterm infant develops ROP. Therefore, it is necessary to identify the onset of ROP in the infants at an early stage, long before it is clinically apparent, by assessing molecular markers from non-invasive ocular fluids.




Europe PMC Funders Author Manuscripts

Recent advancements in the development of electrochemical biosensors [4], [5], [6], [7], [8], florescence-based sensors [9], [10], [11], surface plasmon resonance (SPR)-based biosensors [12], [13], [14] and colorimetric sensors [15], [16] represent a cutting-edge approach for non-invasive monitoring of biomarkers in tear fluids for real-time and continuous health monitoring. A point-of-care diagnostic tool for ROP demands accurate tear-analyte detection in a very small volume, high measurement accuracy, excellent stability, and sensitivity. For this purpose, chemiresistive biosensors [17], [18], [19], [20], [21] detecting tear biomarkers serves as an ideal solution due to its simple design, low cost, rapid response, easy integration with Internet of Things (IoT) systems for remote sensing and data collection, and detection range for very low concentrations of analytes.

Our lab has previously reported several ECM remodelling proteins, particularly MMP-2 and MMP-9, being involved in ROP pathogenesis that can potentially serve as a tear biomarker since their expression varies at different stages of disease development and progression [22], [23], [24]. While assaying the tear in ROP is not an established and routine clinical practice for disease diagnosis, however, there are several reports, including those by our group and others from the literature, that explored the potential benefit of assaying tears for early ROP management [19], [20], [21]. Clinically increased inflammation and angiogenesis in the eye can change or alter the tear film's protein expression, and monitoring these changes in the tear can help monitor the ROP regression and progression [22]; [23]. We have previously [25] reported a chemiresistive biosensor for MMP-9 detection in human tear fluids that demonstrated excellent biosensor performance, such as a wide linear range of operation of the MMP-9 concentration and a very low sub-femto level of target MMP-9 detection. However, the biosensor suffered from poor sensor output response, limiting its resolution and thereby moderate detection accuracy in actual human tears. Vanadium disulfide ($VS_2$) nanowires were selected as the chemi-resistive sensing element owing to their unique combination of metallic conductivity, high surface reactivity, and structural compatibility with functionalization. Unlike semiconducting transition metal dichalcogenides (e.g., $MoS_2$, $WS_2$) [25], $VS_2$ exhibits metallic electronic behavior, which ensures efficient charge transport and low contact resistance, thereby enabling rapid and sensitive signal transduction [26], [27], [28]. The nanowire morphology further enhances the surface-to-volume ratio, providing abundant edge sites and defect states that facilitate strong analyte adsorption and surface redox interactions [24], [29]. Compared to graphene, which often requires additional functionalization to introduce reactivity [30], $VS_2$ intrinsically offers chemically active vanadium and sulfur sites that readily interact with target molecules. Moreover, the sulfur-rich surface allows facile anchoring of thiol-, amine-, or biomolecule-based probes, supporting selective biosensing [31], while the material has demonstrated favorable biocompatibility for integration into bio-interfaces. Collectively, these attributes render $VS_2$ nanowires a superior chemi-resistive sensing platform compared to other 2D materials or nanowires.

Though the utilization of ohmic vanadium disulfide nanowires has presented outstanding prospects of highly sensitive and selective biosensors, the lack of a systematic approach towards biosensor design restricts its full capability towards the determination of bio-analytes in human tears. Sequential surface modifications over the nanomaterial surface are essential for the successful immobilization of antibodies [26]. These layer-by-layer

modifications are nothing, but the chemical treatments subjected to the nanomaterials, ultimately leading to the effective immobilization of antibodies that are functional, stable, and optimally oriented on the sensor surface [27]. The concentration of nanomaterial ink, concentration and incubation time of linker molecules and antibodies, pH of the target analyte solution, and target analyte solution incubation time are the multiple factors involved during the biofunctionalization process [28], [29]. The One Factor at a Time (OFAT) and Trial and Error (TAE) methods are straightforward approaches encompassing the variation of one independent variable while keeping others constant to assess its effect on the sensor performance [30]. This time-consuming repeated experiment execution is resource-intensive and insufficient understanding of the comprehensive multifactorial relationships creates narrow design search space thereby providing suboptimal results. For efficient exploration of design space, more structured computational methods like design of experiments (DoE), machine learning (ML) models, and high-throughput parallel screening are essential for effective experimental design in biosensor development [31].

The unforeseen improvement in the biosensor performance has been observed with the application of Response Surface Methodology (RSM) to the biosensor design and has been increasingly reported in the literature [32], [33], [34]. The Central Composite Design (CCD) has been employed to optimize the design parameters of a florescent miRNA biosensor for cancer diagnosis and exhibited hybridization signal amplification [35]. Another work [36] stated the optimization of padlock probe-based colorimetric bioassay for the detection of G12D KRAS mutation using Plackett-Burman Design (PBD) and RSM. The influence of a systematic experimental approach, increasing the sensitivity and peak current of the analyte, was observed with the development of a cysteamine-linked Fe3O4@Au nanocomposite-based voltametric biosensor for the trinitrotoluene (TNT) detection [37]. The CCD-RSM technique was reported in another work [38] to optimize the surface functionalization method, boosting the sensitivity of a gold nanoparticles/silicon nanowires-based electrochemical biosensor detecting dengue virus DNA oligomers. The RSM technique can adequately model quadratic systems; however, many biosensors' processes might demonstrate more complex, nonlinear relationships that are not well-captured by a quadratic polynomial model [39]. This limitation can be overcome using ML models that have higher efficiency in dealing with high-dimensional spaces, modelling complex and non-linear relationships accurately, and providing more robustness to noise present in the system. Herein, in this study, a CCD and ML-assisted design framework has been developed utilizing a genetic algorithm to provide optimized input factor values to maximize the sensor output signal. Further, the developed chemiresistive tear biochip exhibited an ultra-low limit of detection (LOD) of 0.556 pg/mL, demonstrating its ability to quantify MMP-9 concentration far below the clinically relevant concentration range associated with inflammatory risk in preterm infants. The sensor displayed a broad dynamic range from 1 pg/mL to 50 ng/mL, effectively covering both the normal physiological levels and the elevated concentration range (>10-15 ng/mL) correlated with increased risk of ROP progression. Importantly, the test requires less than 2 μL of tear fluid, aligning with the limited tear volume available in neonates and enabling minimally invasive sampling. The combination of sub-picogram sensitivity, physiologically relevant detection range, and low sample volume requirement confirms the suitability of this biochip for early biochemical

screening of ROP before the manifestation of visible retinal vascular abnormalities. This capability supports its integration into the point-of-care neonatal screening workflows to identify high-risk infants and facilitate timely ophthalmologic intervention.

## II Experimental Section

### A Study Cohort and Clinical Details

A total of 30 preterm (Preterm control-10; Mild ROP-10; Severe ROP-10) infants were recruited and analyzed for the biomarker expression level (Demographic details of the infants in **Table S2**). The ROP diagnosis was made after clinical examination of the fundus by a vitreoretinal specialist using indirect ophthalmoscopy. Preterm infants and ROP cases were diagnosed and categorized based on severity (stages 1-5), location (zones I-III), and extent (clock hours), as well as the presence of “plus” disease, all in accordance with ICROP 3 guidelines ([46]**;** [22]**)**. Severe ROP was defined as aggressive plus disease with significant new vessel growth (stage 3), which can rapidly progress to retinal detachment (stage 4 and 5) if untreated. Hence, prompt early diagnosis and treatment are crucial to prevent progression. Mild ROP was a less severe disease (stages 1 and 2) without “plus” disease or significant new vessel growth. Preterm controls developed a mature retina with complete vascularization, and the retinal vessels were developing normally for the infant’s gestational age. Infants on steroid treatment or with a history of anti-VEGF medication were excluded from the study. The fundus imaging was performed using Optos Silverstone (model name P200TXE, model number A10750). Figure 1 illustrates retinal fundus images from the different stages of ROP, which shows normal complete vascularization among preterm control, minimal tortuosity of vessels in mild ROP infant and increased vascularization showing extensive looping and shunting of vessels with an elevated ridge in zone1 at severe ROP, which could be due to aberrant molecular changes (2, 22). These phenotypes are attributed to the molecular expression of MMP-2, MMP-9, Complement proteins and others, which can be profiled in tears to evaluate the disease severity at an early stage.

### B Design of $VS_2$NW-based biochip platform

**Surface Functionalization method of the $VS_2$NW-based biochip:** To start the biochip preparation, a uniform dispersion of $VS_2$NWs (supplementary material: section 9) was prepared in DI water (5 mg/mL) and dropcasted on the circular active areas of the sensor array. The $VS_2$NWs were dried using substrate thermal treatment as discussed in detail in our previous work to obtain minimum device-to-device variations. The dried layer of the $VS_2$NWs on the gold microelectrodes must undergo sequential surface chemical treatment to functionalize the anti-MMP9 and anti-MMP2 antibodies. To achieve this, the $VS_2$NWs were treated with dimercaptosuccinic acid (MSA) concentrations of 0.1264, 1, 5.5, 10 and 13.0681 mM and incubated for different time durations (3.96, 6, 9, 12 and 14.04 hours). After this, the -COO functional groups were activated using EDC-NHS chemistry by incubating the biochip for 4 hours in a dark place. The activated -CO terminated functional groups were treated with antibody solutions of MMP-9 and MMP-2 of different concentrations (0.1264, 1, 5.5, 10 and 13.0681 μg/mL) overnight for successful biofunctionalization of antibodies on the sensor surface. The unbounded antibody sites were passivated using bovine serum albumin (BSA) solution by incubating for 30 minutes at

37°C. The surface functionalization processes at each step were investigated using Scanning Electron Microscopy (SEM, Zeiss Carl EV018) and electrical resistance was measured for 5 biochips with the help of a Semiconductor Device Analyzer (Agilent B1500).

## III Results and Discussion

### A Surface Functionalization of Biochip

The biofunctionalization process of $VS_2$NWs starts with treating with 2-mercaptosuccinic acid solution. The low dissociation constant $pK_a$ value ($pK_a$ = 3.3) of MSA is because of the dissociation of its carboxyl groups at ph = 7.0 [40]. This allows the MSA molecules to get anchored over the nanowires with correct conformation, with S-H bond getting reacted with vanadium atoms and carboxyl groups are exposed at the top for further surface modifications [41]. The overall surface functionalization at every step is captured using Scanning Electron Microscopy (SEM) images as shown in Figure 2 (II-A). The change in color and size of the $VS_2$NWs after treatment with MSA indicates a successful change in its physicochemical as well as structural properties. The SEM image of $VS_2$NWs after MSA treatment also depicts uniform coating of MSA molecules, essential for more antibodies to get immobilized. Further, the EDC-NHS reaction activates the carboxyl groups using carbodiimide crosslinker chemistry [42]. This entails the abundant primary amines present in the antibody to covalently attach with EDC-NHS activated carboxylic groups (44). This methodology of covalent binding of antibodies with nanomaterial surface provides higher reproducibility, such that the antibodies are immobilized strongly onto the nanowire surface without getting desorbed with changes in pH or ionic changes of the analyte solution [44], [45].

The alteration in electrical properties of the nanowires with each functionalization step is recorded by measuring electrical resistance and shown in Figure 2 (II-B). The electrical resistance was measured for 5 devices at every step of biofunctionalization, and the mean resistance of the nanowires observed was around 30.18 kΩ, owing to their highly conductive nature. After MSA treatment, the self-assembled monolayer (SAM) of the MSA molecule results in an increment of resistance to 3.4 MΩ. The EDC-NHS activation leads to loss of one negative charge per carboxylic group; this interaction further provides a reduction in electrical resistance to 0.314 MΩ. The treatment of EDC-NHS activated $COO^-$ surface with antibody solution forms a covalent bond with the amine groups, resulting in further reduction in the electrical resistance to 0.218 MΩ. The surface mechanistic interpretation of the charge redistribution and dipole orientation at each surface modification step was examined with the zeta potential measurements, and the discussion is provided in the supplementary material (Section 5).

### B ML-assisted framework for biosensor design optimization

**RSM-CCD modelling:** A two-level three-factor CCD was employed to determine the simple and combined effects of three biosensor design variables on the performance of the biosensor. The experimental plan executed using RSM-CCD modelling is explained in detail in the supplementary material (Section 1). The variation in biosensor output response under different biosensor fabrication variable values is presented in Table 1. Statistical testing was

executed for different models with analysis of variance (ANOVA) to examine and predict the desired model and to identify the significant variables. The ANOVA results presented in Table 1 determine the significance of the factors and their interactions affecting the response variables, assess the fit of the fit of CCD model, as well as check for lack of fit. From Table 1, the coded parameters A, B, C, $A^2$, $B^2$ and $C^2$ are significant parameters, i.e., (p>F) <0.05. The correlation coefficient ($R^2$) of 0.9058 stated that 9.42% of the total variations could not be explained using the RSM-CCD model. A high adj-$R^2$ value (near 1.0) is generally expected so that the influence of non-significant terms is minimum. But for this RSM-CCD model, the adj-$R^2$ was 0.8211, which indicates that the model has a moderate influence of non-significant terms and therefore a more accurate model for fitting a non-linear and complex dataset is required. Therefore, the 2D and 3D contour plots presented in Figure 6 **(supplementary material: Section 6)** present sub-optimal results, and a hybrid CCD-SVR-GA model is proposed to precisely model the dataset.

**Hybrid CCD-SVR-GA modelling:** A hybrid approach combining CCD, SVR, and GA offers a powerful framework for optimizing the biosensor construction process, and the flowchart for this hybrid framework is as described in the Figure. 3. The CCD method helps in efficiently exploring the design space and developing an initial response surface model. The first objective of the CCD experimental design is to systematically explore the design space and collect data to build a response surface model as discussed in the **Section 3.2.1**. The main reason for selecting CCD over any other Design of Experiment (DoE) method is the ability to create a quadratic model for the response variable without requiring a full factorial experiment. The experimental data collected from the CCD design is used to train an SVR model. The set of input-output variables (100 in total) generated through collecting results in five replicates for each experimental run from CCD, and the total datapoints were divided into three subsets: training (70%), testing (15%) and cross-validation (15%) from the total datapoints. The hyperparameters of the SVR were tuned using a grid search optimization method, providing the hyperparameter values: C = 100, gamma = 1, kernel = radial basis function (rbf) kernel. The SVR model metrics showed excellent fitting accuracy (training data: $R^2$ = 0.975 and testing data: $R^2$ = 0.966), confirming the modelling accuracy of the non-linear relationships in the dataset.

The evolutionary algorithms like GA have superior performance and therefore used to search the design space using the SVR model as the objective function. The GA optimization iteratively evolves a population of candidate solutions through selection, crossover, and mutation, guided by the predictions from the SVR model. The computational parameters of the GA used in the process of biosensor optimization of enhanced signal amplification: population size: 100, elite ratio: 0.01, crossover fraction: 0.9, number of generations: 400, fitness scaling function: rank fitness scaling, and selection function: stochastic uniform. The implementation of GA with these computational parameters resulted in the convergence of the objective function after 2 iterations. The hybrid CCD-SVR-GA model yielded optimised biosensor fabrication parameters: an MSA incubation time of 9 hours, an MSA concentration for uniform coating of MSA over $VS_2$NWs of 5.75 mM, and a monoclonal anti-MMP9 antibody concentration required for high-density antibody immobilisation of 5.26 μg/mL. The maximised sensor response (ΔR/R) obtained with this hybrid CCD-SVR-

GA model was 5.14, and the experimental result (ΔR/R = 5.29) validated the model's response.

**$VS_2$NWs-based biosensor calibration and performance:** The VS2NWs-based biosensor was fabricated using the optimized parameters obtained from the hybrid CCD-SVR-GA model as mentioned in Section Hybrid CCD-SVR-GA modelling. The standard calibration curves for MMP-9 and MMP-2 tear proteins are provided in Figure 4 (A) and (B), respectively. The standard curve was calibrated for MMP-9 concentration from 1 pg/mL to 50 ng/mL for MMP-9 bioassay, and the standard curve was calibrated for MMP-2 concentration from 10 pg/mL to 100 ng/mL for the MMP-2 bioassay. The limit of detection (LOD) for the MMP-9 and MMP-2 bioassay was found to be 0.556 pg/mL and 0.605 pg/mL, respectively, computed using the LOD formula given by:

$$LOD = Mean\ of\ blank\ PBS\ solution + (1.645 \times\ Standard\ deviation\ of\ the\ lowest\ protein\ concentration)$$

The interference studies for MMP-9 and MMP-2 bioassay are presented in Figure 4 (C) and (D), respectively, which clearly show very minimum cross-reactivity with other tear proteins such as Immunoglobulin A (IgA), lysozyme, C-reactive protein (CRP), complement component 3 (C3), and complement component 3-A (C3a). Among all the tear proteins, the interference studies have demonstrated that the lysozyme of 1 ng/mL concentration exhibited a ΔR/R of 1.85 and 1.98 for the MMP-9 and MMP-2 bioassay, respectively. The IEP of lysozyme is between 10.5 to 12 [46] and gets positively charged when exposed to a pH medium of 7.4 and therefore gets electrostatically attracted to the negatively charged bioassays. Still, the target MMP-9 and MMP-2 proteins have a much higher response (ΔR/R) than all other tear proteins and therefore have very less foul response from the tear fluid. The stability studies for the MMP-9 and MMP-2 bioassays are depicted in Figure 4 (E) and (F), respectively, executed by storing the bioassays at 4°C for seven weeks in a sealed petridish. The stability studies for both the bioassays show very little degradation in the sensor response for over seven weeks, thereby confirming the robustness and reliability of the bioassays to be used in a clinical setup.

**Expression of MMP-9 and MMP-2 in tears using ELISA and $VS_2$NW-based biochip:** Next, after biosensor design and optimization, we compared the MMP-2 and MMP-9 expression using ELISA and biochip in ROP tears. An increasing trend in MMP-9 concentration was observed in ROP groups as compared to the pre-term control group in biochip as well as ELISA; however, for MMP-2, the concentration was found to be decreased in the case of severe ROP as compared to pre-term control (Figure 5A). Further, a significant decrease in MMP-2 concentrations was observed in ELISA readings as compared to nano-sensors in pre-term controls and the case of mild ROP category (*p-value* ≤0.05) (Figure 5B). These changes can be attributed to better antibody immobilization and optimization in biosensors. The degree of variation was also minimal in the biosensor as compared to ELISA in the ROP category. The MMP9 data observed using ELISA and nano-sensor in this study collaborated well with our previous report on increased levels of MMP9 in both the vitreous humor and tears of severe ROP infants [22], [23]. The MMP-9 levels are higher at the mild stage itself, which could be the driver for the severe stage and

thus can serve as a better marker for ROP. Our enhanced and better-optimized biosensor can also be used for various other biomarkers across different diseases, including diabetic retinopathy, dry eye, AMD and others, and it gives a lesser margin of error, thus increasing reliability and accuracy.

**Expression of MMP-9 and MMP-2 in tear at different stages of ROP in biosensor and ELISA:** We next analyzed the expression level of MMPs in the different stages of ROP under both nano-sensor and ELISA. While both nano-sensor and ELISA were able to distinguish the control vs ROP category, however, the significant increase in MMP-9 concentration was observed in biosensor (*p-value-0.008*) as compared to ELISA (*p-value-0.032*). Further, on stratifying the ROP group into mild and severe ROP, the nano-sensor showed a significant increase in MMP-9 concentrations in both mild ($p<0.01$) and severe ROP ($p<0.05$) groups as compared to their pre-term controls (Figure 6B), whereas no significant change in categories was observed in ELISA (Figure 6A).

With these concentration levels of MMP-9, we speculate that preterm infants at having MMP-9 concentrations at the control or mild stage are at risk of developing of severe ROP. The concentration of MMP-9 quantified using biosensor (Control-8.46 ng/mL; mild ROP-15.71 ng/mL; severe ROP-14.88 ng/mL) and ELISA (Control-4.18 ng/mL; mild ROP-9.19 ng/mL; severe ROP-8.77 ng/mL) showed similar trend and fold increment. This biosensor, designed especially for ROP diagnosis, can reliably identify these infants at high risk of progression and can be given early medical intervention. The difference in ELISA and sensor reading can be due to the fact the ELISA kit comes for multiple analytes (in this case MMP-9 and MMP-2), since both MMPs are isoforms of the same protein, this is easily impacted by the competitive binding of antigen and antibody. The other reason could be the difference in the antibody sequence used for ELISA and biosensor. Further, the increased expression level in biosensors can be due to the better design of our CCD model and ML-based approach. MMP-2 expression was inconsistent as reported above (supplementary file). It is noteworthy that some of the control infants progressed to the mild stage and a few mild-stage infants progressed to the severe stage, we observed that MMP-9 expression in such cases increased in comparison to the infants who did not progress. However, due to the limited sample size of progressed and non-progressed infants, we need to validate this in a larger sample cohort.

**Receiver Operator Characteristics (ROC) for MMPs using Biosensor and ELISA expression profile:** The sensitivity and specificity of the expression of MMP-9 and MMP-2 were studied using the ROC curve and the area under the curve (AUC). The AUC for MMP-9 expression using biosensor was 0.97 with high sensitivity (100%) and specificity (96.67%) while AUC for MMP-9 expression using ELISA was 0.82 with specificity of 70.3% and sensitivity of 100% (Figure 7).

Both MMP2 and MMP9 are critical zinc-dependent enzymes that degrade the ECM, a process essential for both healthy tissue remodelling and retinal pathological conditions like ROP with increased angiogenesis and inflammation. Inhibiting MMPs can reduce retinal neovascularization in an oxygen-induced retinopathy (OIR) model [54]. Expression of MMP9 and MMP2 in vitreous humor (VH) of ROP infants shows their high activity at

severe ROP [19]. We have shown in an earlier report using an in-vitro cellular system that increased MMP9 expression under hypoxic conditions degrades the protein opticin in the VH of ROP patients [21], which is successfully rescued by inhibiting MMP activity using doxycycline. Our studies shows that levels of MMP9 are significantly elevated in mild and severe ROP cases, while MMP2 does not show a significant difference among the tears of the infants. MMP9 can be considered a better clinical indicator and a more significant contributor to the disease's progression. This is because MMP9 has a higher enzymatic activity and can break down a wider range of ECM substrates compared to MMP2 [55]. This higher efficiency of MMP9 in degrading the ECM facilitates the abnormal new blood vessel growth and retinal detachment characteristic of severe ROP.

## IV Conclusion

The study highlights significant improvement in biosensor optimization, which could enhance the accuracy, sensitivity, and specificity of the MMP quantification for point-of-care diagnosis in regular clinical use for ROP. The current study has demonstrated the capability of non-invasive molecular biomarkers to differentiate preterm infants with and without ROP along the progression of disease. We could have studied the correlation of fundus images of the subject recruited in the study with biosensor reading, but this was not performed due to the unavailability of fundus images especially for no-ROP and mild ROP cases. Despite this the significant differences detected by the biosensor between mild and severe ROP cases underscore its utility in risk stratification and timely intervention. A rigorous assessment biosensor demonstrated higher sensitivity and specificity (AUC-0.97) compared to traditional ELISA methods (AUC-0.82), highlighting its potential for early detection and monitoring of ROP from small volume of tear (as ELISA requires higher tear quantity).

## Acknowledgment

The authors thank the parents of all the preterm and full-term babies for their voluntary participation.

### Funding Information

This work was partly supported by a COE grant (BT/PR32404/MED/30/2136/2019) from the Department of Biotechnology, IMPRINT grant (IMP/2018/001414) from the Ministry of Human Resource and development-Department of Science and Technology-Govt. of India, and Hyderabad Eye Research Foundation. SK is supported through the Department of Biotechnology, Government of India fellowship (DBT/2020/LVPEI/1365). AM is supported through the DBT India Alliance grant (IA/E/22/1/506766).

## References

[1]. Rivera, JC, , et al. BioMed Central Ltd; 2017 Aug 22. Retinopathy of prematurity: Inflammation, choroidal degeneration, and novel promising therapeutic strategies.

[2]. Kaur, T, Patnaik, S, Kumar, S, Kaur, I. Genetics of Ocular Diseases. Nema, N, Nema, HV, editors. Springer Nature Singapore; Singapore: 2022. 101–123.

[3]. Hartnett, ME. Elsevier Inc; 2015 Jan 01. Pathophysiology and mechanisms of severe retinopathy of prematurity.

[4]. Rotake DR, Ghosh TN, Singh SG. Tear-Based Electrochemical Sensor for Detecting Complement III Protein Using Indium-Doped Zinc Oxide Nanofibers with Superior Dielectric Properties. IEEE Sens Lett. 2023; Nov; 7 (11) 1–4. DOI: 10.1109/LSENS.2023.3326465 [PubMed: 37529707]

[5]. Rotake DR, Ghosh TN, Singh SG. Electrochemical nano-biosensor based on electrospun indium zinc oxide nanofibers for the determination of complement component 3 protein. Microchimica Acta. 2023; Aug. 190 (8) [PubMed: 37490230]

[6]. Yan Q, Peng B, Su G, Cohan BE, Major TC, Meyerhoff ME. Measurement of tear glucose levels with amperometric glucose biosensor/capillary tube configuration. Anal Chem. 2011; Nov; 83 (21) 8341–8346. [PubMed: 21961809]

[7]. Sempionatto JR, et al. Eyeglasses-based tear biosensing system: Non-invasive detection of alcohol, vitamins and glucose. Biosens Bioelectron. 2019; Jul. 137: 161–170. DOI: 10.1016/j.bios.2019.04.058 [PubMed: 31096082]

[8]. Xu J, Tao X, Liu X, Yang L. Wearable Eye Patch Biosensor for Noninvasive and Simultaneous Detection of Multiple Biomarkers in Human Tears. Anal Chem. 2022; Jun; 94 (24) 8659–8667. [PubMed: 35656772]

[9]. Shi Y, et al. Smartphone-based fluorescent sensing platforms for point-of-care ocular lactoferrin detection. Sens Actuators B Chem. 2023; Mar. 378 doi: 10.1016/j.snb.2022.133128

[10]. Zhang Y, Yan P, Tang H, Zhang J. Rapid detection of tear lactoferrin for diagnosis of dry eyes by using fluorescence polarization-based aptasensor. Sci Rep. 2023; Dec. 13 (1) doi: 10.1038/s41598-023-42484-5 [PubMed: 37704755]

[11]. Shi, Y, Hu, Y, Jiang, N, Yetisen, AK. American Chemical Society; 2022 Jun 24. Fluorescence Sensing Technologies for Ophthalmic Diagnosis.

[12]. Park M, Jung H, Jeong Y, Jeong KH. Plasmonic Schirmer Strip for Human Tear-Based Gouty Arthritis Diagnosis Using Surface-Enhanced Raman Scattering. ACS Nano. 2017; Jan; 11 (1) 438–443. [PubMed: 27973769]

[13]. Kim S, et al. Label-Free Surface-Enhanced Raman Spectroscopy Biosensor for On-Site Breast Cancer Detection Using Human Tears. ACS Appl Mater Interfaces. 2020; Feb; 12 (7) 7897–7904. [PubMed: 31971765]

[14]. Culver HR, Wechsler ME, Peppas NA. Label-Free Detection of Tear Biomarkers Using Hydrogel-Coated Gold Nanoshells in a Localized Surface Plasmon Resonance-Based Biosensor. ACS Nano. 2018; Sep; 12 (9) 9342–9354. DOI: 10.1021/acsnano.8b04348 [PubMed: 30204412]

[15]. Park S, et al. Cerium Oxide Nanoparticle-Containing Colorimetric Contact Lenses for Noninvasively Monitoring Human Tear Glucose. ACS Appl Nano Mater. 2021; May; 4 (5) 5198–5210. DOI: 10.1021/acsanm.1c00603

[16]. Kang BH, Park M, Jeong KH. Colorimetric Schirmer strip for tear glucose detection. Biochip J. 2017; Dec; 11 (4) 294–299. DOI: 10.1007/s13206-017-1405-7

[17]. Supraja P, Tripathy S, Govind Singh S. Smartphone-powered, ultrasensitive, and selective, portable and stable multi-analyte chemiresistive immunosensing platform with PPY/COOH-MWCNT as bioelectrical transducer: Towards point-of-care TBI diagnosis. Bioelectrochemistry. 2023; Jun. 151 [PubMed: 36805206]

[18]. Zhou J, et al. A high sensitive chemiresistive-biosensor based on self-assembly grown GaN porous layer. Sens Actuators B Chem. 2021; Oct. 345 doi: 10.1016/j.snb.2021.130360

[19]. Bangar MA, Shirale DJ, Chen W, Myung NV, Mulchandani A. Single conducting polymer nanowire chemiresistive label-free immunosensor for cancer biomarker. Anal Chem. 2009; Mar; 81 (6) 2168–2175. [PubMed: 19281260]

[20]. Bangar MA, Shirale DJ, Chen W, Myung NV, Mulchandani A. Single conducting polymer nanowire chemiresistive label-free immunosensor for cancer biomarker. Anal Chem. 2009; Mar; 81 (6) 2168–2175. DOI: 10.1021/ac802319f [PubMed: 19281260]

[21]. Tripathy S, Bhandari V, Sharma P, Vanjari SRK, Singh SG. Chemiresistive DNA hybridization sensor with electrospun nanofibers: A method to minimize inter-device variability. Biosens Bioelectron. 2019; May. 133: 24–31. [PubMed: 30903938]

[22]. Rathi S, et al. Abnormal complement activation and inflammation in the pathogenesis of retinopathy of prematurity. Front Immunol. 2017; Dec. 8 doi: 10.3389/fimmu.2017.01868 [PubMed: 29312345]

[23]. Patnaik S, et al. An interplay of microglia and matrix metalloproteinase MMP9 under hypoxic stress regulates the opticin expression in retina. Sci Rep. 2021; Dec. 11 (1) doi: 10.1038/s41598-021-86302-2 [PubMed: 33811221]

[24]. Kumar S, et al. Arachidonic acid metabolism regulates the development of retinopathy of prematurity among preterm infants. J Neurochem. 2024; 168 (9) 3171–3187. DOI: 10.1111/jnc.16190 [PubMed: 39073120]

[25]. Ghosh TN, Rotake D, Kumar S, Kaur I, Singh SG. Tear-based MMP-9 detection: A rapid antigen test for ocular inflammatory disorders using vanadium disulfide nanowires assisted chemi-resistive biosensor. Anal Chim Acta. 2023; Jul. 1263 [PubMed: 37225335]

[26]. Woeppel KM, Zheng XS, Cui XT. Enhancing surface immobilization of bioactive molecules via a silica nanoparticle based coating. J Mater Chem B. 2018; 6 (19) 3058–3067. DOI: 10.1039/C8TB00408K [PubMed: 30464839]

[27]. Bilal, M, Qamar, SA, Berenguer-Murcia, Á, Fernandez-Lafuente, R. Elsevier Inc; 2024 Jan 01. Proteases immobilized on nanomaterials for biocatalytic, environmental and biomedical applications: Advantages and drawbacks.

[28]. Purohit, B, Vernekar, PR, Shetti, NP, Chandra, P. KeAi Communications Co; 2020 Jan 01. Biosensor nanoengineering: Design, operation, and implementation for biomolecular analysis.

[29]. Kalita, N, Gogoi, S, Minteer, SD, Goswami, P. American Chemical Society; 2023 Dec 20. Advances in Bioelectrode Design for Developing Electrochemical Biosensors.

[30]. Bhaturiwala R, Bagban M, Mansuri A, Modi H. Successive approach of medium optimization using one-factor-at-a-time and response surface methodology for improved β-mannanase production from Streptomyces sp. Bioresour Technol Rep. 2022; Jun. 18 doi: 10.1016/j.biteb.2022.101087

[31]. Cao, B, , et al. American Chemical Society; 2018 Aug 28. How to optimize materials and devices via design of experiments and machine learning: Demonstration using organic photovoltaics.

[32]. Mirmoghtadaie L, Ensafi AA, Kadivar M, Norouzi P. Highly selective electrochemical biosensor for the determination of folic acid based on DNA modified-pencil graphite electrode using response surface methodology. Materials Science and Engineering C. 2013; Apr; 33 (3) 1753–1758. [PubMed: 23827633]

[33]. Gouda MD, Karanth NG. Optimization of the multienzyme system for sucrose biosensor by response surface methodology.

[34]. Rizi KS, et al. Response surface methodology optimized electrochemical DNA biosensor based on HAPNPTs/PPY/MWCNTs nanocomposite for detecting Mycobacterium tuberculosis. Talanta. 2021; May. 226 [PubMed: 33676656]

[35]. El Aamri M, Zayani R, Baachaoui S, Mohammadi H, Amine A, Raouafi N. An ingenious double-amplified fluorometric genosensor based on hybridization chain reaction and enzymatic signal for the sensitive detection of piRNA–651. Sens Actuators B Chem. 2024; Jan. 399 doi: 10.1016/j.snb.2023.134749

[36]. Mahmoudian F, et al. Designing A Fluorescence Padlock Probe-Based Biosensor and Colorimetric Assay For The Detection of G12D KRAS Mutation. Biomark Med. 2021; Dec; 15 (18) 1741–1754. [PubMed: 34784779]

[37]. Soltani-Shahrivar M, Afkhami A, Madrakian T. Design and optimization of a cost-effective paper-based voltammetric sensor for the determination of trinitrotoluene (TNT) utilizing cysteamine-linked Fe3O4 @Au nanocomposite. Talanta. 2024; Jul. 274 [PubMed: 38581854]

[38]. Abdul Rashid JI, Yusof NA, Abdullah J, Hashim U, Hajian R. Surface modifications to boost sensitivities of electrochemical biosensors using gold nanoparticles/silicon nanowires and response surface methodology approach. J Mater Sci. 2016; Jan; 51 (2) 1083–1097. DOI: 10.1007/s10853-015-9438-6

[39]. Mowbray M, et al. Machine learning for biochemical engineering: A review. Biochem Eng J. 2021; Aug. 172 doi: 10.1016/j.bej.2021.108054

[40]. Królikowska A, Bukowska J. Self-assembled monolayers of mercaptosuccinic acid on silver and gold surfaces designed for protein binding. Part I: Structure of the monolayer. Journal of Raman Spectroscopy. 2007; 38 (7) 936–942. DOI: 10.1002/jrs.1741

[41]. Królikowska A, Bukowska J. Self-assembled monolayers of mercaptosuccinic acid monolayers on silver and gold surfaces designed for protein binding. Part II: Vibrational spectroscopy studies on cytochrome c immobilization. Journal of Raman Spectroscopy. 2007; 38 (7) 943–949. DOI: 10.1002/jrs.1739

[42]. Cammarata CR, Hughes ME, Ofner CM. Carbodiimide induced cross-linking, ligand addition, and degradation in gelatin. Mol Pharm. 2015; Mar; 12 (3) 783–793. DOI: 10.1021/mp5006118 [PubMed: 25658665]

[43]. Asiaei S, Smith B, Nieva P. Enhancing conjugation rate of antibodies to carboxylates: Numerical modeling of conjugation kinetics in microfluidic channels and characterization of chemical over-exposure in conventional protocols by quartz crystal microbalance. Biomicrofluidics. 2015; Nov. 9 (6) doi: 10.1063/1.4937929 [PubMed: 26697125]

[44]. Batalla P, Fuentes M, Mateo C, Grazu V, Fernandez-Lafuente R, Guisan JM. Covalent immobilization of antibodies on finally inert support surfaces through their surface regions having the highest densites in carboxyl groups. Biomacromolecules. 2008; Aug; 9 (8) 2230–2236. [PubMed: 18558741]

[45]. Zhu X, Xiong S, Zhang J, Zhang X, Tong X, Kong S. Improving paper-based ELISA performance through covalent immobilization of antibodies. Sens Actuators B Chem. 2018; Feb. 255: 598–604. DOI: 10.1016/j.snb.2017.08.090

[46]. Sarkar S, Saikia A, Kundu S. Effect of ions on the adsorption of lysozyme protein below its isoelectric point on hydrophilic (OH-Si) and hydrophobic (H-Si) surfaces. New Journal of Chemistry. 2023; May; 47 (27) 12697–12708. DOI: 10.1039/d3nj00624g

Europe PMC Funders Author Manuscripts

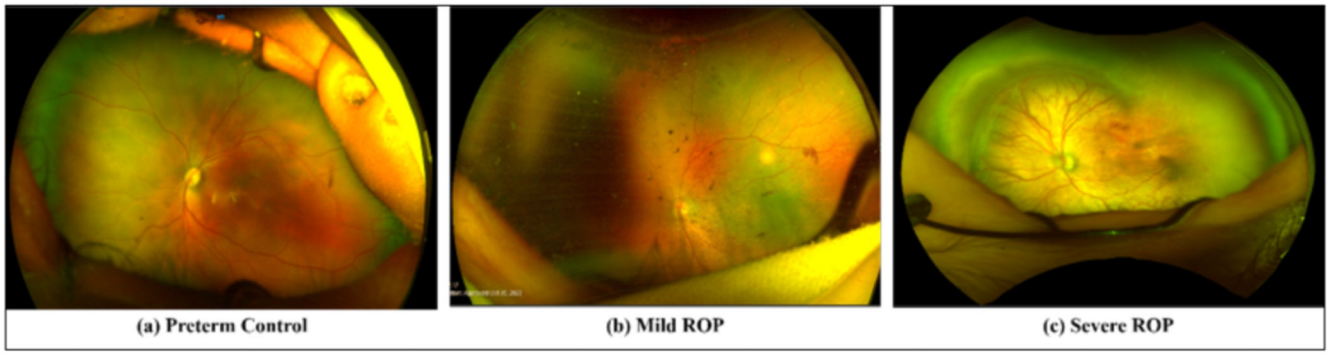


**Figure 1.**

Retinal Fundus Imaging: The fundus images of left eye of the infants recruited for the study showing different stages of ROP. Ultra-wide field fundus image showing preterm control (a) normal complete vascularisation till the periphery; mild (b)): showing minimal tortuosity of vessels in the temporal quadrant with an early ridge formation suggestive of zone2, stage 2 ROP and severe ROP (c) showing extensive looping and shunting of vessels with an elevated ridge in zone1 suggestive of aggressive retinopathy of prematurity. The fundus imaging was performed using Optos Silverstone (model name P200TXE, model number A10750). The Optos Silverstone produces a 200-degree single capture image in <0.4 seconds. The images are pseudo-colour with red and green channel separation.

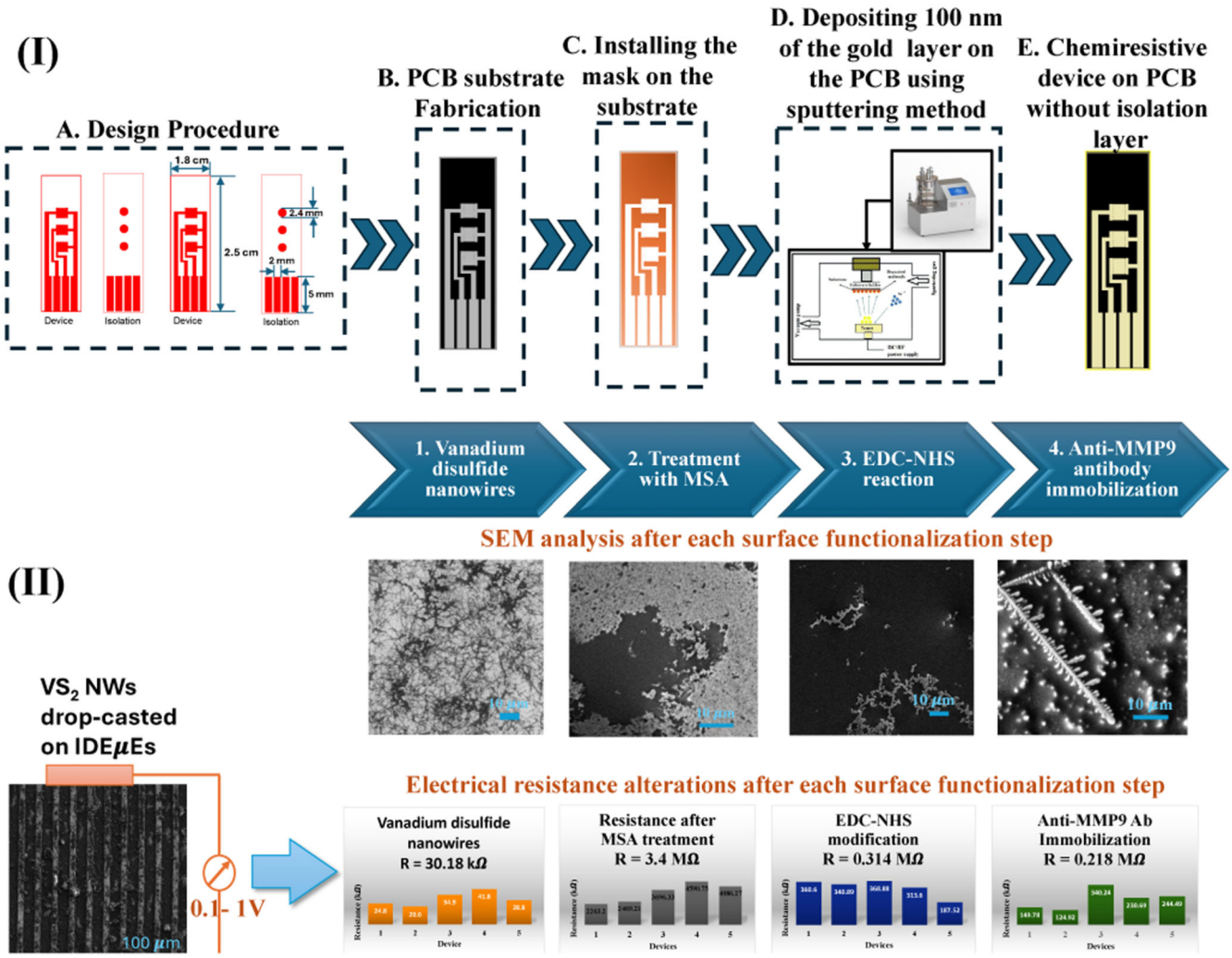


**Figure 2.**

(I) Workflow of biochip fabrication methodology; (II) (A) Scanning Electron Microscopy (SEM) images of overall surface functionalization at every step and (B) Electrical resistance obtained after each surface functionalization step for five sensors.

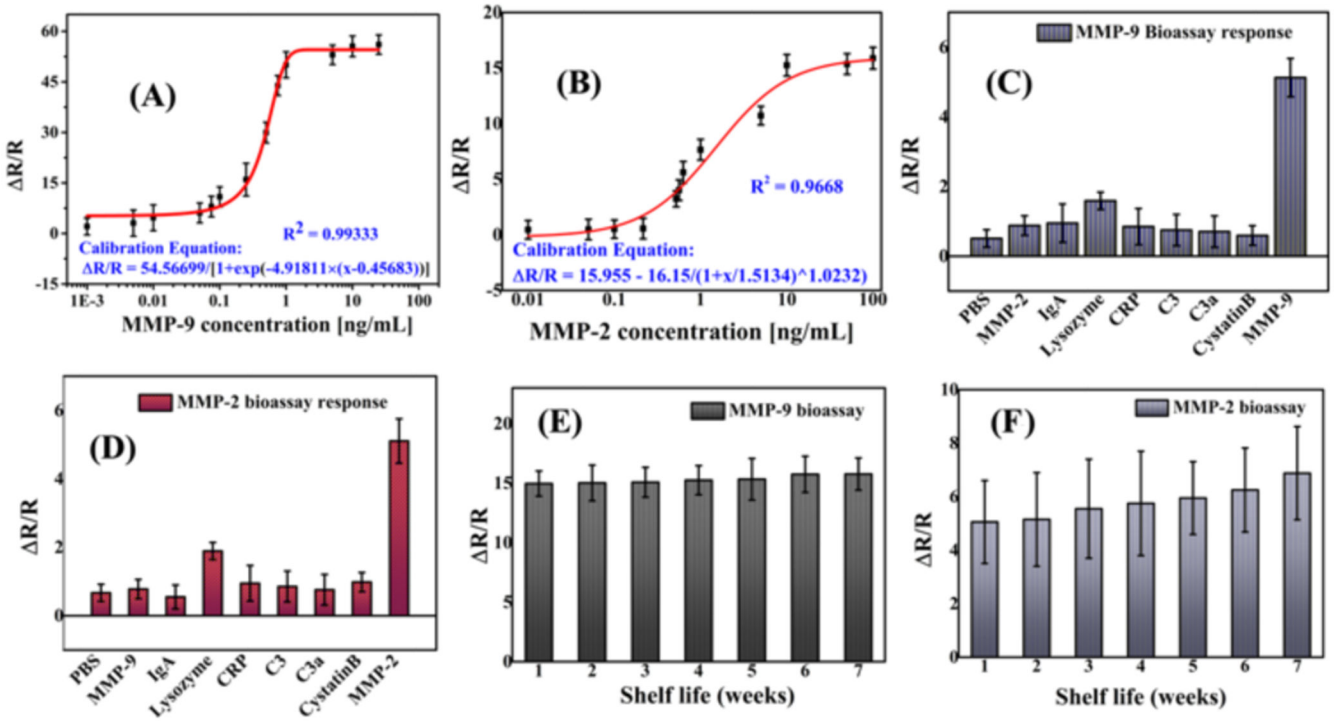


**Figure 3.**

Calibration plots for (A) MMP-9 and (B) MMP-2 bioassay; Interference study for (C) MMP-9 and (D) MMP-2 bioassay; and stability study for (E) MMP-9 and (F) MMP-2 bioassay.





Europe PMC Funders Author Manuscripts

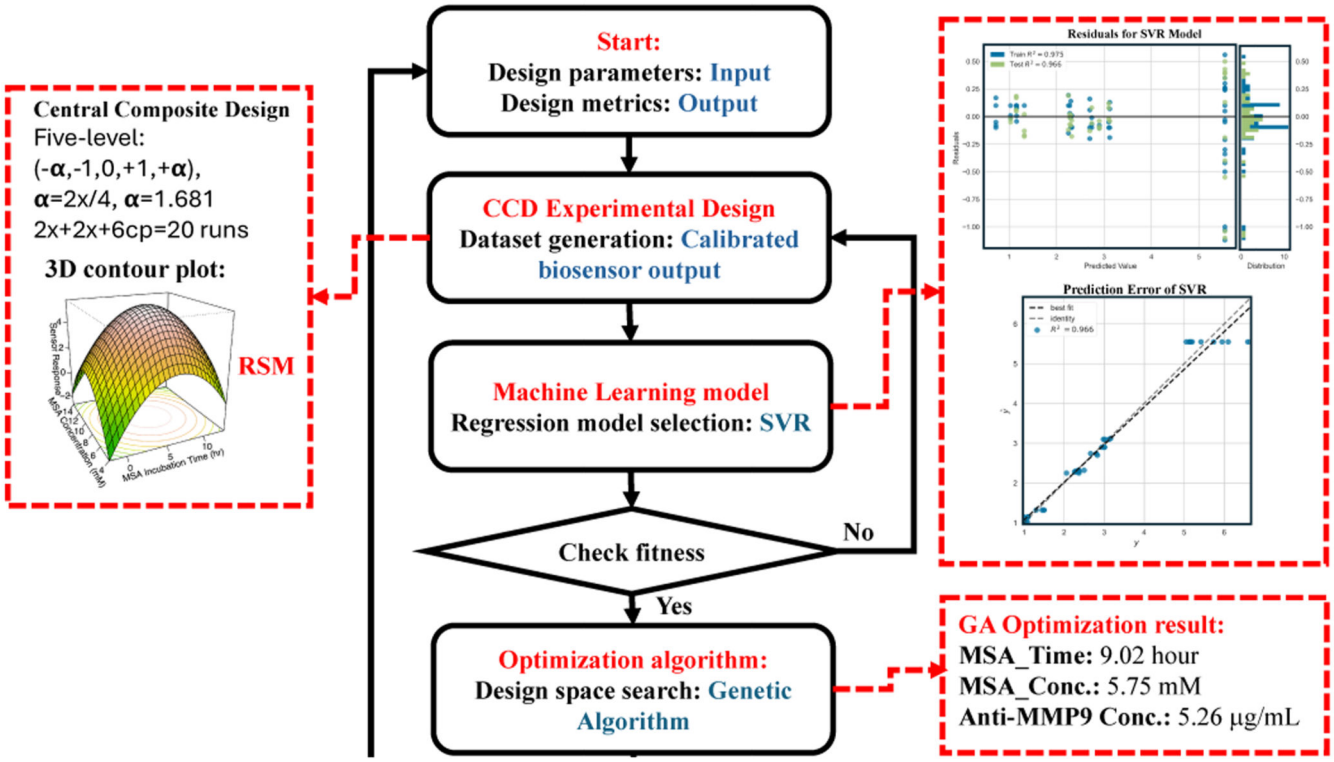


**Figure 4.**
Central Composite Design (CCD) with Support Vector Regression (SVM) framework described as a flowchart.




Europe PMC Funders Author Manuscripts

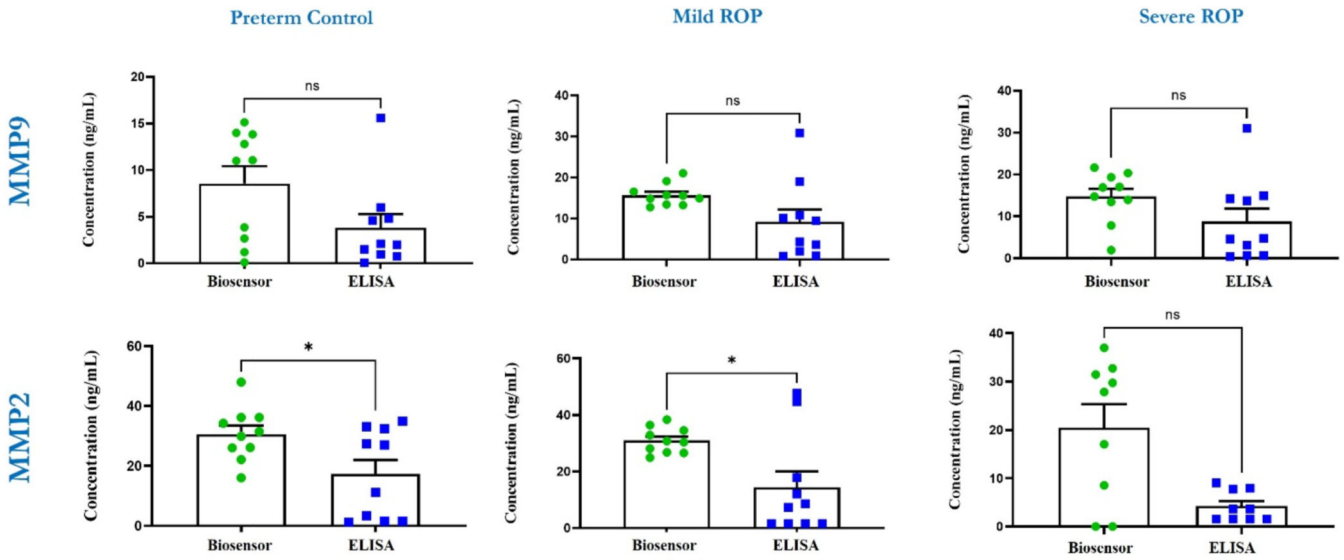


**Figure 5.**

The comparison of concentration levels of MMP-9 and MMP-2 across different stages of ROP infants using both biosensor and commercially available ELISA kits. The data is presented as mean ± SD (N =30).

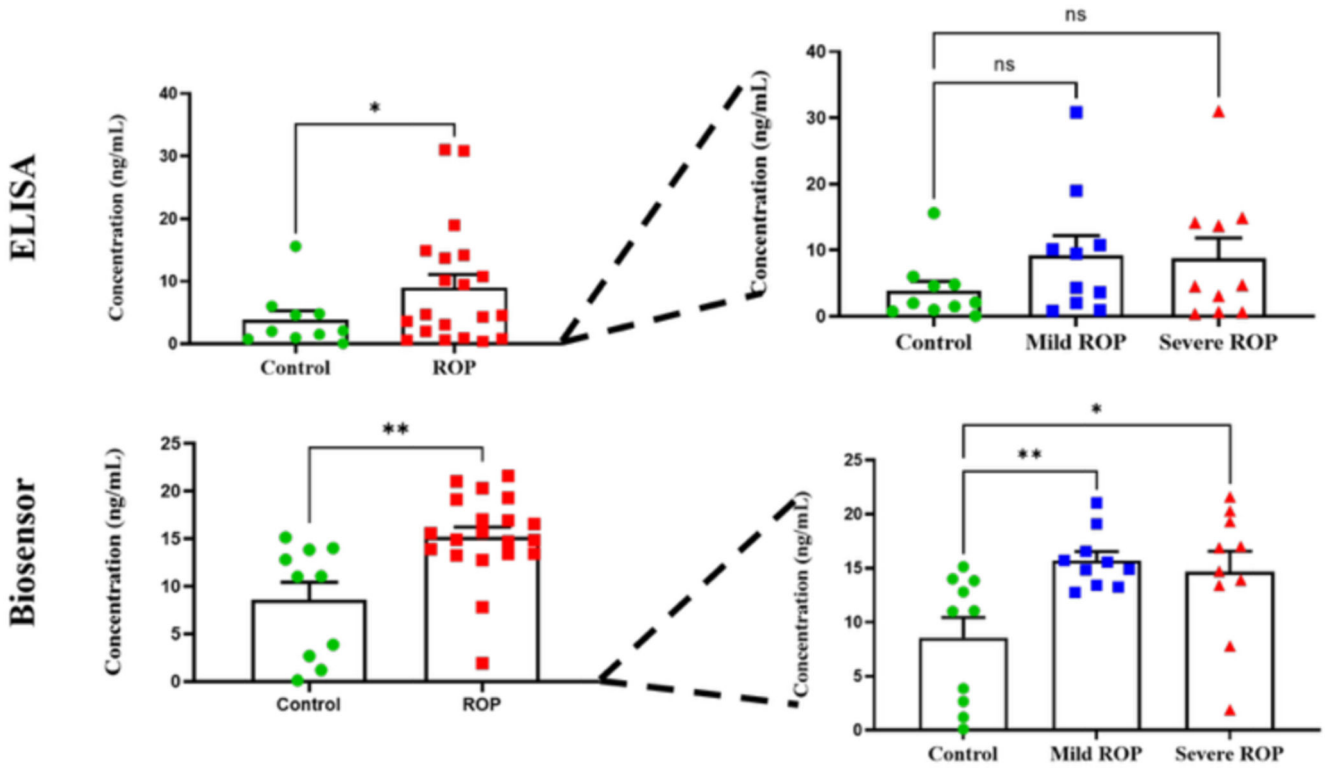


**Figure 6.**

The MMP-9 expression profile across different stages of ROP using ELISA (A) and biosensor (B) The MMP-9 shows significant increase among ROP vs preterm control cases, and this change is implicated across control, mild ROP, and severe ROP. *<0. 05, **p<0.01.




Europe PMC Funders Author Manuscripts

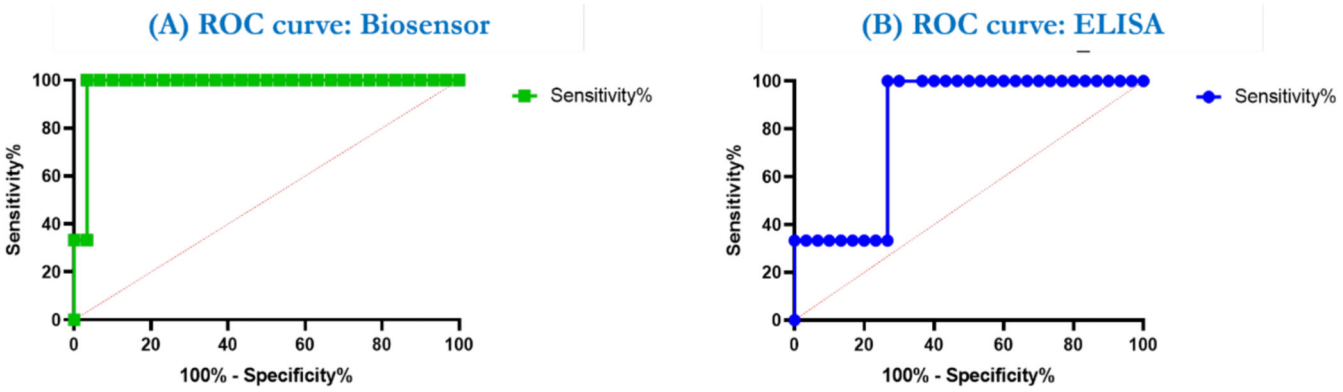


**Figure 7.**

The ROC curve of MMP-9 expression using both (A) biosensor (AUC-0.9778; p-value-<0.0001; standard error-0.022); Optimal threshold-1.0, Youden Index-96.67 (B) ELISA (AUC-0.8228; p-value-<0.0001; standard error-0.058), optimal threshold-1.25, Youden Index-70.37.

Europe PMC Funders Author Manuscripts

**Table 1 Analysis of variance (ANOVA) results for the RSM-CCD model**

| | Estimate | Std. Error | t Value | Pr (>\|t\|) |
|---|---|---|---|---|
| **Intercept** | -11.0102 | 2.4636680 | | |
| **MSA_T (A)** | 2.6894 | 0.4537 | 5.9266 | 0.0001457*** |
| **MSA C (B)** | 0.8374 | 0.23626 | 3.544 | 0.00531** |
| **Ab_C (C)** | 0.6709055 | 0.2362678 | 2.8396 | 0.01756 * |
| **MSA_T: MSA_C (AB)** | -0.0140 | 0.02074 | -0.6761 | 0.5143161 |
| **MSA_T:Ab _C (AC)** | -0.0045 | 0.0207484 | -0.2200 | 0.8302915 |
| **MSA_C:Ab C_(BC)** | 0.01201 | 0.01383 | 0.8689 | 0.4052869 |
| **MSA_T$^2$ (A$^2$)** | -0.1446438 | 0.0232253 | -6.2278 | 9.783e-05*** |
| **MSA_C$^2$ (B$^2$)** | -0.0648985 | 0.0103224 | -6.2872 | 9.058e-0.5 *** |
| **Ab_C$^2$ (C$^2$)** | -0.0537881 | 0.0103224 | -5.2108 | 0.0003951 *** |